Eur. Phys. J. C (2009) 61: 711–720
DOI 10.1140/epjc/s10052-009-0878-5

THE EUROPEAN PHYSICAL JOURNAL C

Regular Article - Experimental Physics

NA60 results on thermal dimuons

NA60 Collaboration

R. Arnaldi[11], K. Banicz[4,6], K. Borer[1], J. Castor[5], B. Chaurand[9], W. Chen[2], C. Cicalò[3], A. Colla[11], P. Cortese[11], S. Damjanovic[4,a], A. David[4,7], A. de Falco[3], A. Devaux[5], L. Ducroux[8], H. En'yo[10], J. Fargeix[5], A. Ferretti[11], M. Floris[3], A. Förster[4], P. Force[5], N. Guettet[4,5], A. Guichard[8], H. Gulkanian[12], J.M. Heuser[10], M. Keil[4,7], L. Kluberg[9], Z. Li[2], C. Lourenço[4], J. Lozano[7], F. Manso[5], P. Martins[4,7], A. Masoni[3], A. Neves[7], H. Ohnishi[10], C. Oppedisano[11], P. Parracho[4,7], P. Pillot[8], T. Poghosyan[12], G. Puddu[3], E. Radermacher[4], P. Ramalhete[4,7], P. Rosinsky[4], E. Scomparin[11], J. Seixas[7], S. Serci[3], R. Shahoyan[4,7], P. Sonderegger[7], H.J. Specht[6], R. Tieulent[8], G. Usai[3], R. Veenhof[7], H.K. Wöhri[3,7]

[1]Laboratory for High Energy Physics, Bern, Switzerland
[2]BNL, Upton, NY, USA
[3]Università di Cagliari and INFN, Cagliari, Italy
[4]CERN, Geneva, Switzerland
[5]LPC, Université Blaise Pascal and CNRS-IN2P3, Clermont-Ferrand, France
[6]Physikalisches Institut der Universität Heidelberg, Heidelberg, Germany
[7]IST-CFTP, Lisbon, Portugal
[8]IPN-Lyon, Univ. Claude Bernard Lyon-I and CNRS-IN2P3, Lyon, France
[9]LLR, Ecole Polytechnique and CNRS-IN2P3, Palaiseau, France
[10]RIKEN, Wako, Saitama, Japan
[11]Università di Torino and INFN, Torino, Italy
[12]YerPhI, Yerevan, Armenia

Received: 14 September 2008 / Revised: 16 December 2008 / Published online: 10 February 2009

Abstract The NA60 experiment at the CERN SPS has measured muon pairs with unprecedented precision in 158 A GeV In–In collisions. A strong excess of pairs above the known sources is observed in the whole mass region $0.2 < M < 2.6$ GeV. The mass spectrum for $M < 1$ GeV is consistent with a dominant contribution from $\pi^+\pi^- \rightarrow \rho \rightarrow \mu^+\mu^-$ annihilation. The associated ρ spectral function shows a strong broadening, but essentially no shift in mass. For $M > 1$ GeV, the excess is found to be prompt, not due to enhanced charm production, with pronounced differences to Drell–Yan pairs. The slope parameter $T_{\rm eff}$ associated with the transverse momentum spectra rises with mass up to the ρ, followed by a sudden decline above. The rise for $M < 1$ GeV is consistent with radial flow of a hadronic emission source. The seeming absence of significant flow for $M > 1$ GeV and its relation to parton–hadron duality is discussed in detail, suggesting a dominantly partonic emission source in this region. A comparison of the data to the present status of theoretical modeling is also contained. The accumulated empirical evidence, including also a Planck-like shape of the mass spectra at low p_T and the lack of polarization, is consistent with a global interpretation of the excess dimuons as thermal radiation. We conclude with first results on ω in-medium effects.

PACS 25.75.-q · 12.38.Mh · 13.85.Qk

1 Introduction

Dileptons are particularly attractive to study the hot and dense QCD matter formed in high-energy nuclear collisions. In contrast to hadrons, they directly probe the entire space–time evolution of the expanding system, escaping freely without final-state interactions. At low masses $M < 1$ GeV (LMR), thermal dilepton production is mediated by the broad vector meson ρ (770) in the hadronic phase. Due to its strong coupling to the $\pi\pi$ channel and the short life time of only 1.3 fm/c, "in-medium" modifications of its mass and width close to the QCD phase boundary have since long been considered as the prime signature for *chiral symmetry restoration* [1–3]. At intermediate masses $M > 1$ GeV (IMR), it has been controversial up to today whether thermal dileptons are dominantly produced in

[a] e-mail: sanja.damjanovic@cern.ch

the earlier partonic or in the hadronic phase, based here on hadronic processes other than $\pi\pi$ annihilation. Originally, thermal emission from the early phase was considered as a prime probe of *deconfinement* [4, 5].

Experimentally, it took more than a decade to master the challenges of very rare signals and enormous combinatorial backgrounds. The first clear signs of an excess of dileptons above the known decay sources at SPS energies were obtained by CERES [6, 7] for $M < 1$ GeV, NA38/NA50 [8] for $M > 1$ GeV and by HELIOS-3 [9] for both mass regions (see [10] for a short recent review including the preceding pp era and the theoretical milestones). The sole existence of an excess gave a strong boost to theory, with hundreds of publications. In the LMR region, $\pi\pi$ annihilation with regeneration and strong in-medium modifications of the intermediate ρ during the fireball expansion emerged as the dominant source. However, the data quality in terms of statistics and mass resolution remained largely insufficient for a precise assessment for the in-medium spectral properties of the ρ. In the IMR region, thermal sources or enhanced charm production could account for the excess equally well, but that ambiguity could not be resolved, nor could the nature of the thermal sources be clarified.

A big step forward in technology, leading to completely new standards of the data quality in this field, has recently been achieved by NA60, a third-generation experiment built specifically to follow up the open issues addressed above [11]. Initial results on mass and transverse momentum spectra of the excess dimuons have already been published [11–13], supplemented by recent results on acceptance-corrected mass spectra and polarization [14]. This paper takes a broader view on the results, discussing in some detail the observed M–p_T correlations, the connection to hadron–parton duality, and the present status of theoretical modeling. Certain aspects of the p_T spectra, of centrality dependencies and evidence for ω in-medium effects are reported here for the first time.

2 Mass spectra and the ρ spectral function

Figure 2.1 shows the centrality-integrated net dimuon mass spectrum for 158 A GeV In–In collisions in the LMR region. The narrow vector mesons ω and ϕ are completely resolved; the mass resolution at the ω is 20 MeV. The peripheral data can be completely described by the electromagnetic decays of neutral mesons [12, 15]. This is not true for the more central data as plotted in Fig. 2.1, due to the existence of a strong excess of pairs. The high data quality of NA60 allows to isolate this excess with a priori *unknown characteristics* without any fits: the cocktail of the decay sources is subtracted from the total data using *local* criteria, which are solely based on the mass distribution itself. The ρ is not subtracted. The excess resulting from this difference formation

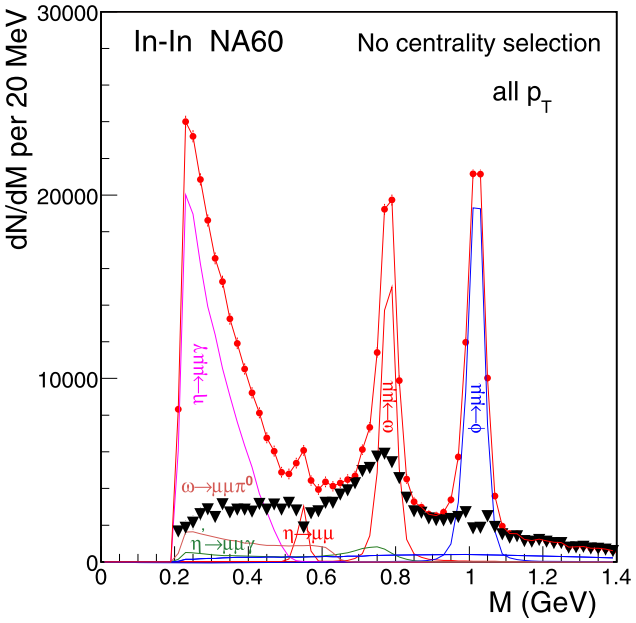

Fig. 2.1 Background-subtracted mass spectrum before (*dots*) and after subtraction of the known decay sources (*triangles*)

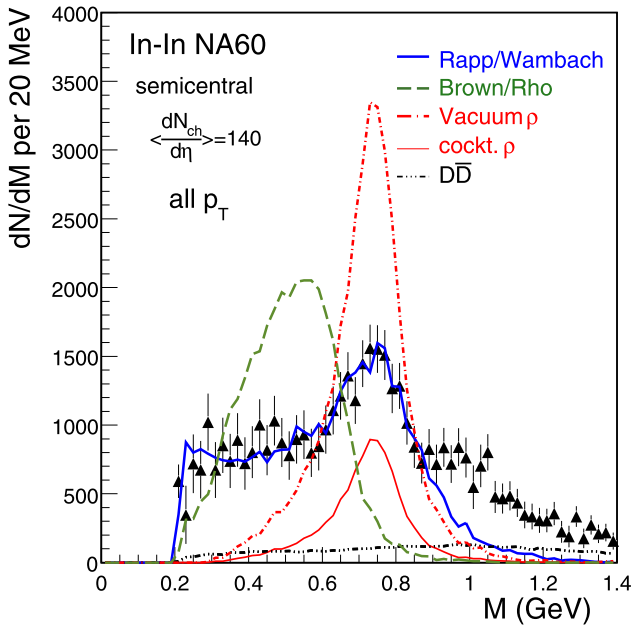

Fig. 2.2 Excess dimuons compared to theoretical predictions [16], renormalized to the data in the mass interval $M < 0.9$ GeV. No acceptance correction applied

is illustrated in the same figure (see [12, 13, 15] for details and error discussion). The subtracted data for the η, ω and ϕ themselves are subject to the same further steps as the excess data and are used later for comparison.

The common features of the excess mass spectra can be recognized in Fig. 2.2. A peaked structure is always seen, residing on a broad continuum with a yield strongly increas-

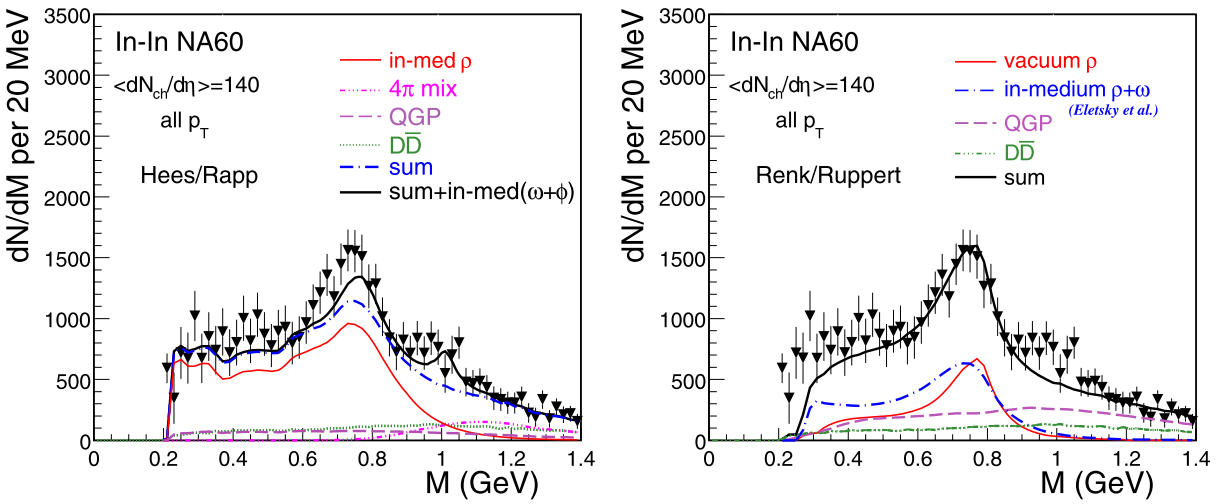

Fig. 2.3 Excess dimuons for semicentral collisions compared to the theoretical model results by Hees/Rapp [18] (*left*) and Renk/Ruppert et al. [19] (*right*). No acceptance correction applied

ing with centrality (see Fig. 4.6 below), but remaining essentially centered around the nominal ρ pole [15]. Without any acceptance correction and p_T selection, the data can directly be interpreted as the *space–time averaged spectral function* of the ρ, due to a fortuitous cancellation of the mass and p_T dependence of the acceptance filtering by the phase space factors associated with thermal dilepton emission [15]. The two main theoretical scenarios for the in-medium spectral properties of the ρ, broadening [2] and dropping mass [3], are shown for comparison, both evaluated for the same fireball evolution [16]. Since agreement between modeling and data would imply agreement both in shape and yield, the model results are normalized to the data in the mass interval $M < 0.9$ GeV, just to be independent of the uncertainties of the fireball evolution. The unmodified ρ, also shown in Fig. 2.2 (vacuum ρ), is clearly ruled out. The broadening scenario indeed gets close, while the dropping mass scenario in the version which described the CERES data reasonably well [2, 3, 6] completely fails for the much more precise NA60 data. A strong reduction of in-medium VMD as proposed by the vector manifestation of chiral symmetry [17] would make hadron spectral functions in hot and dense matter altogether unobservable, but central aspects of this scenario are totally unclear, and quantitative predictions which could be confronted with data have not become available up to today.

A comparison of the same excess mass spectrum to two more recent theoretical developments, covering now both the LMR and the initial part of the IMR region, is contained in Fig. 2.3. In contrast to Fig. 2.2, the theoretical results are not renormalized here, but shown on an absolute scale. In the ρ-like region with $\pi^+\pi^- \to \rho \to \mu^+\mu^-$ as the dominant source, Hees/Rapp [18] use the original many-body scenario with a ρ spectral function strongly broadened by baryonic interactions [2], while Renk/Ruppert's results [19] are based on the spectral function of Eletsky et al. [20] where the broadening effects from baryons are somewhat weaker; that difference is directly visible in the low-mass tails of the theoretical mass spectra. The overall agreement between the data and the two theoretical scenarios is quite satisfactory in this region, also in absolute terms.

3 Mass spectra and parton–hadron duality

Moving up into the IMR region $M > 1$ GeV, 2π processes become negligible, and other hadronic processes like 4π (including vector–axialvector mixing in case of [18]) and partonic processes like quark–antiquark annihilation $q\bar{q} \to \mu^+\mu^-$ take over. The two theoretical scenarios in Fig. 2.3 also describe this part. However, there is a very interesting and instructive difference between them. While the total yield of the data for $M > 1$ GeV is described about equally well, the fraction of partonic processes relative to the total is small in [18] where a first-order phase transition is used, and dominant in [19] which uses a cross-over phase transition. This feature is often referred to as "parton–hadron duality" and formed the basis of the successful description of the NA50 dimuon enhancement in the IMR region in terms of thermal radiation [21]. Here, the individual sources were not even specified.

Caution should, however, be expressed as to the use of the term "duality" in this context. Parton–hadron duality is a statement on dilepton emission *rates*, dating back to the time-reversed process of hadron production in e^+e^- collisions. It implies that the emission rates using either partonic (pQCD) or hadronic degrees of freedom merge together, i.e. become "dual", if the system approaches deconfinement and

chiral restoration. The validity of duality down to masses of 1 GeV, mainly due to vector–axialvector mixing, was first shown by Li and Gale [22] (see also [2]). However, experiments measure *yields*, i.e. rates integrated over space–time. Duality in the yields is not obvious and becomes questionable, if the space–time trajectories are *different* for genuine partonic and hadronic processes. Such a difference automatically appears through the elementary assumption that partonic processes only act "early", i.e. from $T_{\rm i}$ until $T_{\rm c}$, while hadronic processes (like $n\pi$) only act "late", i.e. from $T_{\rm c}$ to thermal freeze-out $T_{\rm f}$. If theoretical scenarios are *different* in their trajectories (both as to partonic and to hadronic processes), the integrated total yields will, in general, be different. Since the scenarios of [18] and [19] in Fig. 2.3 are indeed very different (see above), the seemingly equivalent description of the data cannot be traced to duality, but must be due to internal parameter choices.

Explicit insight beyond duality, be it real or fortuitous, can be obtained experimentally in the following way (see [5] and in particular [23]). In contrast to real photons, virtual photons decaying into lepton pairs are characterized by two variables, mass M and transverse momentum p_T. Historically, the interest has largely focused on mass because of its rich and often structured information content, including now the ρ spectral function discussed above. Transverse momentum, on the other hand, contains not only contributions from the spectral function(s), but encodes the key properties of the expanding fireball, temperature and, in particular, transverse (radial) flow. The latter causes a blue shift of p_T, analogous to the case of hadrons. In contrast to hadrons, however, which always receive the full asymptotic flow reached at the moment of decoupling from the flowing medium, lepton pairs are continuously emitted during the evolution, reflecting a space–time folding over the temperature-flow history in their final p_T spectra. Since flow builds up monotonically during the evolution, being small in the early partonic phase (at SPS energies, due to the "soft point" in the equation-of-state), and increasingly larger in the late hadronic phase, the final p_T spectra keep memory on the *time ordering* of the different dilepton sources, mirrored in a characteristic *mass dependence of the p_T spectra*. We shall come back to this point below.

4 Acceptance-corrected mass and p_T spectra

Quantitative insight into the physical meaning of the excess dileptons requires a full correction of the data for geometrical acceptance and pair efficiencies of the NA60 apparatus, including the effects of the trigger system. Results from Monte Carlo simulations of the acceptance are contained in [13, 24], showing significant variations and in particular a strong decrease at low mass and low p_T. In principle, the correction requires a 4-dimensional grid in the space of $M - p_T - y - \cos\theta_{\rm CS}$ (where $\theta_{\rm CS}$ is the polar angle of the muons in the Collins Soper frame). To avoid large statistical errors in low-acceptance bins, it is performed instead in 2-dimensional M–p_T space, using the measured y and $\cos\theta$ distributions as an input. The latter are, in turn, obtained with acceptance corrections determined in an iterative way from MC simulations matched to the data in M and p_T. The y-distribution is found to have the same rapidity width as $\mathrm{d}N_{\rm ch}/\mathrm{d}\eta$, $\sigma_y \sim 1.5$ [24]. The $\cos\theta_{\rm CS}$ distributions for two mass windows of the excess and the ω are contained in [14]. Within errors, they are found to be uniform, implying the polarization of the excess dimuons to be zero, in contrast to Drell–Yan and consistent with the expectations for thermal radiation from a randomized system.

The outcome for the two major variables M and p_T is first discussed separately for the LMR and the IMR regions. Figure 4.1 shows a set of mass spectra for some selected slices in p_T to illustrate the evolution from low to high p_T (a p_T-integrated mass spectrum over the whole mass region is contained in [11]). The spectra are normalized to $\mathrm{d}N_{\rm ch}/\mathrm{d}\eta$ in absolute terms, using the same procedure as described in detail for the ϕ in [25] and relating $N_{\rm part} \simeq \mathrm{d}N_{\rm ch}/\mathrm{d}\eta$ at $\eta = 2.9$ as measured to within 10% by the *Si* pixel telescope. Recent theoretical results on thermal radiation from three major groups working in the field are included for comparison [18, 19, 23, 26, 27], calculated absolutely (not normalized to the data). Results from a fourth one [28] only cover the 2π region and are not yet available in p_T-differential form. The general agreement between data and model results both as to spectral shapes and to absolute yields is most remarkable, supporting the term "thermal" used throughout this paper.

At very low p_T, a strong rise towards low masses is seen in the data, reflecting the Boltzmann factor, i.e. the Plank-like radiation associated with a very broad, nearly flat spectral function. Only the Hees/Rapp scenario [26] is able to describe this part quantitatively, due to their particularly large contribution from baryonic interactions to the low-mass tail of the ρ spectral function (as in [28]). This was already mentioned in connection with Fig. 2.3, but is much more clearly visible at low p_T than without any p_T selection. At higher p_T, the influence of radial flow increasingly changes the spectral shapes, and at very high p_T all spectra appear ρ-like. However, sizable differences between the different theoretical scenarios also exist in this region. For example, Hees/Rapp [26] use a hard-scattering ρ which contributes to fill up the ρ region beyond the Cooper–Frye freeze-out ρ. They also use an extrapolation of the Drell–Yan process down to the photon point ($M \to 0$). While this contribution is small for the whole LMR region without p_T selection, the low-mass/high-p_T part is in their case completely dominated by DY. The size of radial flow, the major issue here,

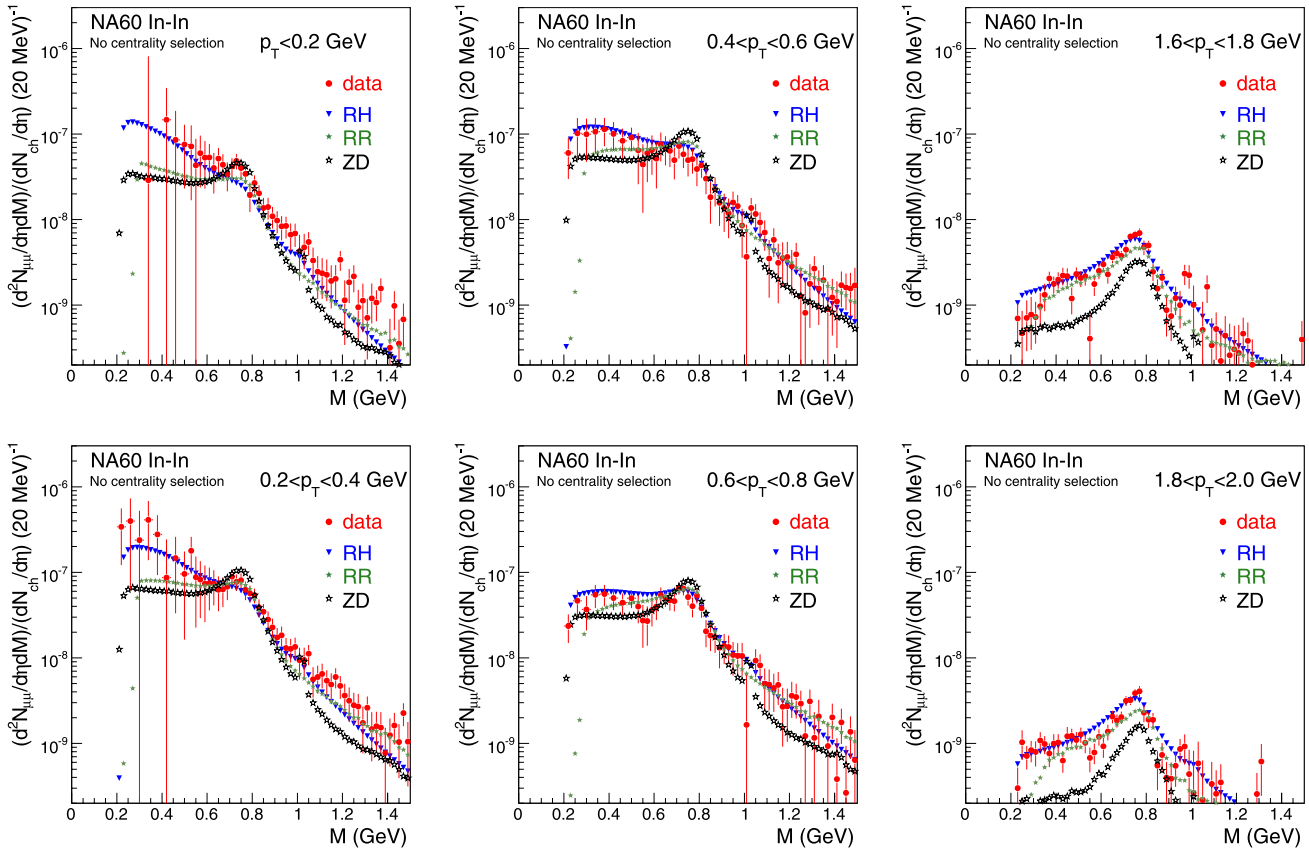

Fig. 4.1 Acceptance-corrected mass spectra of the excess dimuons in selected slices of p_T. Absolute normalization as in Fig. 4.1. The theoretical scenarios are labeled according to the authors HR [26], RR [23], and ZD [27]. In case of [26], the EoS-B$^+$ option is used, leading to a partonic fraction of about 65% in the IMR (different from the left part of Fig. 2.3)

also varies between the three groups. It is recognizably too low in the hydrodynamics scenario [27], and maximal for the fireball scenario of [19, 23] tailored to the NA60 hadron data.

Figure 4.2 (left) shows the centrality-integrated m_T spectra, where $m_T = (p_T^2 + M^2)^{1/2}$, for four mass windows; the ϕ is included for comparison. The ordinate is absolutely normalized to $\mathrm{d}N_{\mathrm{ch}}/\mathrm{d}\eta$ as in Fig. 4.1. Apart from a peculiar rise at low m_T (<0.2 GeV) for the excess spectra (not the ϕ) which only disappears for very peripheral collisions [10, 13], all spectra are pure exponentials. The rise is outside of any systematic errors as discussed in [13]. The relative yield associated with it is about 10–20%, roughly independent of mass, which excludes a connection to the low p_T rise seen in pion p_T spectra. The absolute yield steeply decreases with mass, reminiscent of Dalitz decays. However, a consistent physical interpretation is still open. The lines in the exponential region are fits to the data with the function $1/m_T\,\mathrm{d}N/\mathrm{d}m_T \propto \exp(-m_T/T_{\mathrm{eff}})$, where the effective temperature parameter T_{eff} is the inverse slope of the distributions. For the excess data, the fits are restricted to the range $0.4 < p_T < 1.8$ GeV (roughly $0.1 < m_T - M < 1.2$ GeV) to exclude the increased rise at low m_T. Obviously, the slopes depend on mass. Figure 4.2 (right) shows a more detailed view into the ρ-like mass window, exploiting the same side-window method as used in connection with Fig. 4.6 below, to determine the p_T spectra separately for the ρ peak and the underlying continuum. All spectra are purely exponential up to the cut-off at $p_T = 3$ GeV, without any signs of an upward bend characteristic for the onset of hard processes. Their slopes are, however, quite different (see below).

The central NA60 results in the IMR region [11] are shown in Fig. 4.3. The use of the *Si*-vertex tracker allows to measure the offset between the muon tracks and the main interaction vertex and thereby to disentangle prompt and offset dimuons from D decays. The offset distribution is found to be perfectly consistent with no charm enhancement, expressed by a fraction of 1.16 ± 0.16 of the level expected from upscaling the NA50 results on the IMR in p–A collisions [11]. The observed excess is really prompt, with an enhancement over Drell–Yan by a factor of 2.4 ± 0.08. The excess can now be isolated in the same way as was done in the LMR region, subtracting the measured known sources,

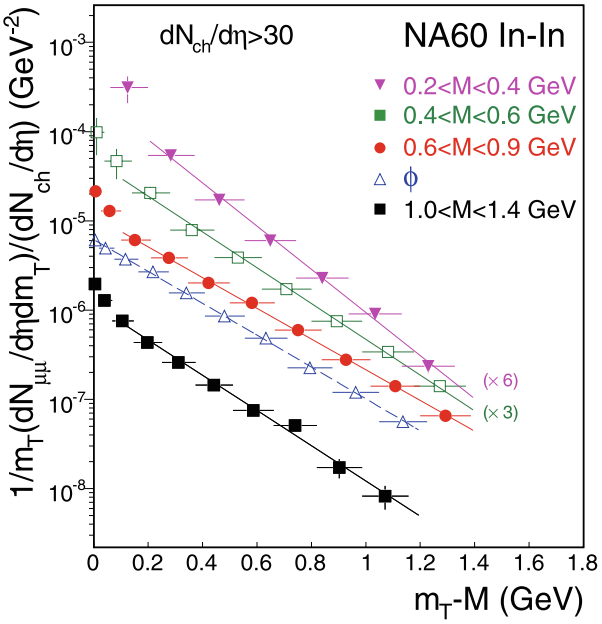

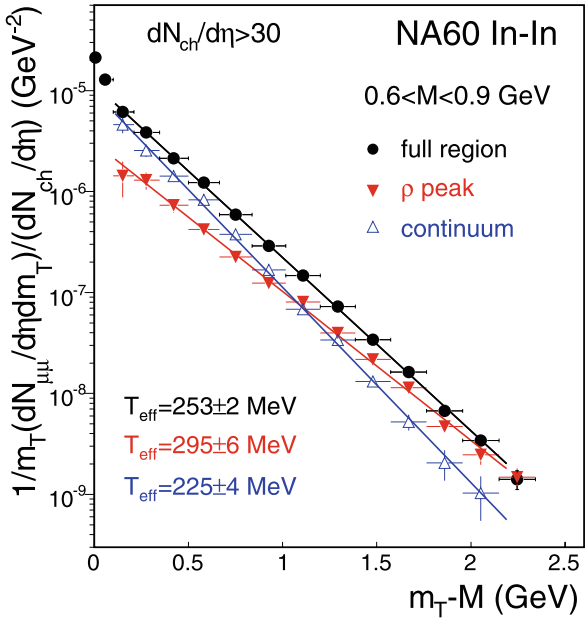

Fig. 4.2 Acceptance-corrected transverse mass spectra of the excess dimuons for 4 mass windows and the ϕ [13] (*left*), and a decomposition into peak and continuum for the ρ-like window (*right*, see text). *Open charm* is subtracted throughout. The normalization in absolute terms is independent of rapidity over the region measured. For error discussion see [13]

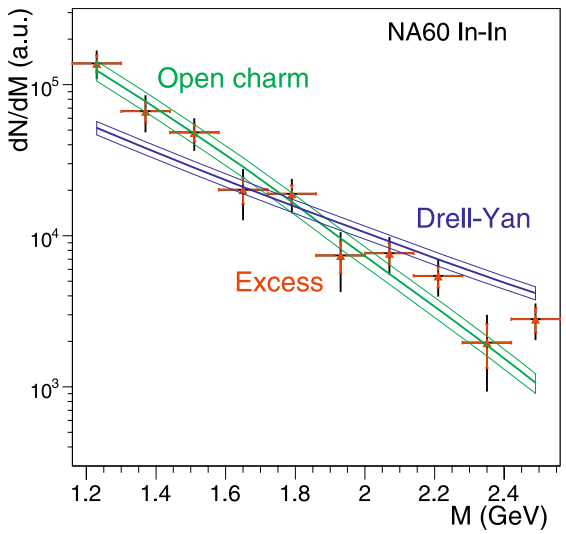

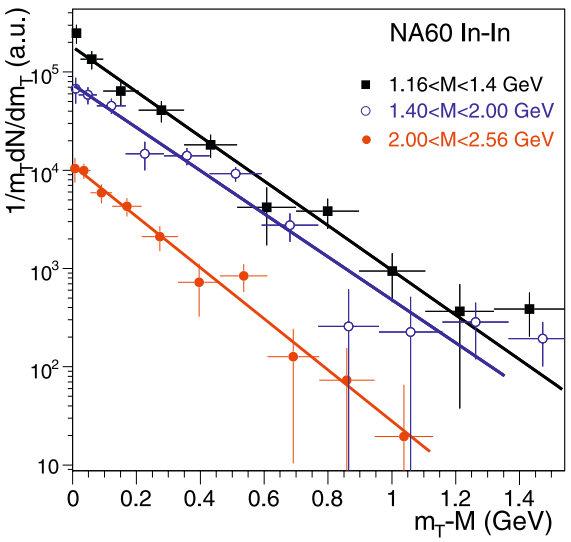

Fig. 4.3 Acceptance-corrected mass spectra of all three contributions to the IMR spectrum: Drell–Yan, *open charm* and the excess (*triangles*). The data are integrated over centrality

Fig. 4.4 Acceptance-corrected transverse mass spectra of the excess dimuons for three mass windows. The data are integrated over centrality. For error discussion see [11]

here DY and open charm, from the total data. Figure 4.3 shows the decomposition of the total into DY, open charm and the prompt excess. The mass spectrum of the excess is quite similar to the shape of open charm and much steeper than DY; this explains of course why NA50 could describe the excess as enhanced open charm [8].

The transverse momentum spectra are also much steeper than DY. Moreover, the spectra depend on mass and do not show the factorization between mass and p_T characteristic for DY, where a common Gaussian distribution with a fixed sigma $k_T = 0.8$ GeV describes all p_T spectra independent of mass. The transverse mass spectra are shown in Fig. 4.4 for three consecutive mass windows. All spectra are essentially exponential. However, the steepening observed at very low m_T in the lowest mass window, seen already before for all masses in Fig. 4.2 including this window, seems to be switched-off in the upper two mass windows. As in Fig. 4.2,

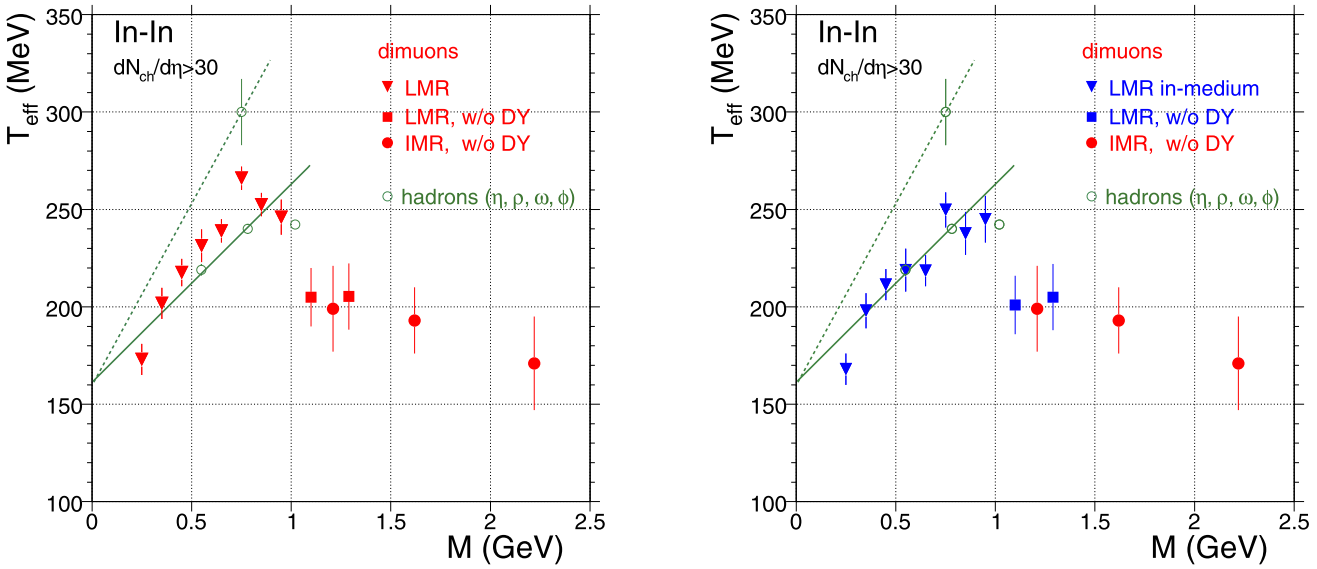

Fig. 4.5 *Left*: Inverse slope parameter T_{eff} vs. dimuon mass for the combined LMR/IMR regions of the excess in comparison to hadrons [13]. *Right*: Inverse slope parameters T_{eff} for the "pure" in-medium part, obtained by subtraction of the ρ-peak contribution from the total before the fits are done (see text). *Open charm* is subtracted throughout. Errors in the LMR part are purely statistical; the systematic errors are mostly smaller than the statistical ones [13]. Errors in the IMR part are total errors [11]

the lines are exponential fits to the data, restricted again to $p_T \geq 0.5$ GeV to exclude the rise at low m_T. The extracted inverse slope parameters are 199 ± 21 (stat) ± 3 (syst), $193 \pm 16 \pm 2$ and $171 \pm 21 \pm 3$ MeV, respectively, i.e. about the same within the (rather large) errors.

The inverse slope parameters T_{eff} extracted from the exponential fits to the m_T spectra are plotted in the left panel of Fig. 4.5 vs. dimuon mass, unifying the data from the LMR and IMR regions. In the LMR part, a finer binning is used than in Fig. 4.2, and the coarser-binned data (contained in [13]) are left out for clarity. For $M < 1$ GeV, a correction for Drell–Yan pairs is not done, due to their small contribution [13] and the intrinsic uncertainties at low masses [26]. In the extended LMR analysis up to 1.4 GeV, the 2 (square) points are corrected, as are all points of the IMR analysis (see above). In the region of overlap, the data are not statistically independent. The hadron data for η, ω and ϕ obtained as a by-product of the cocktail subtraction procedure are also included in Fig. 4.5, as is the single value for the ρ-peak from the right panel of Fig. 4.2. Interpreting the latter as the freeze-out ρ without in-medium effects, consistent with all present theoretical modeling [18, 19, 23, 26, 27], all four hadron values together with preliminary π^- data from NA60 can be subjected to a simple blast wave analysis [14]. This results in a reasonable set of freeze-out parameters of the fireball evolution and suggests the following consistent interpretation for the hadron and dimuon data together. Maximal radial flow is reached by the ρ, due to its maximal coupling to pions, while all other hadrons follow some hierarchy in earlier freeze-out. The T_{eff} values of the dimuon excess rise nearly linearly with mass up to the pole position of the ρ, but stay always well below the ρ line, completely *consistent* with the expectations for *radial flow* of an *in-medium hadron-like* source (here $\pi^+\pi^- \rightarrow \rho$) decaying continuously into lepton pairs.

This picture can still be refined. By modeling a ρ with the proper spectral shape and the m_T spectrum as measured, its contribution can be subtracted from the total measured distribution in the full M–m_T plane with the same side-window method as used for Fig. 4.6 below and described in [15]. The difference, essentially a continuum, is then refit, resulting in T_{eff} values for the "pure" *in-medium* (continuum) part in the 2π region. The modified plot is shown in the right panel of Fig. 4.5. The appearance is striking: all values are lower, but mostly so in the bin associated with the ρ pole (by $\sim$20 MeV). This makes the shape even more sawtooth-like than before, and within errors the rise continues now up to about 1 GeV.

Beyond the 2π region, the T_{eff} values of the excess dimuons show a sudden decline by about 50 MeV down to the IMR values. This decline is even more abrupt in the right panel of Fig. 4.5 than in the left and obviously connected to the in-medium emission itself, not to any peculiarities associated with the ρ peak. Extrapolating the lower-mass trend set by a hadron-like source to beyond 1 GeV, such a fast transition is extremely hard to reconcile with emission sources which continue to be of dominantly hadronic origin in this region. A much more natural explanation would be a transition to a dominantly early, i.e. *partonic* emission source

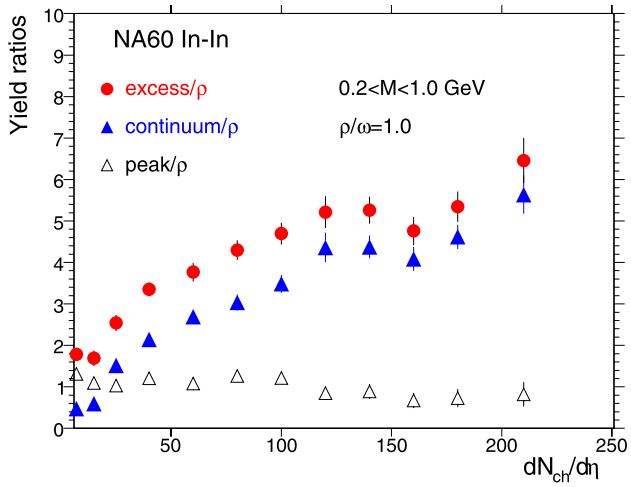

Fig. 4.6 Excess yield ratios for peak, continuum and total vs. centrality for the mass window $0.2 < M < 1$ GeV. *Open charm* is subtracted throughout. No acceptance correction applied

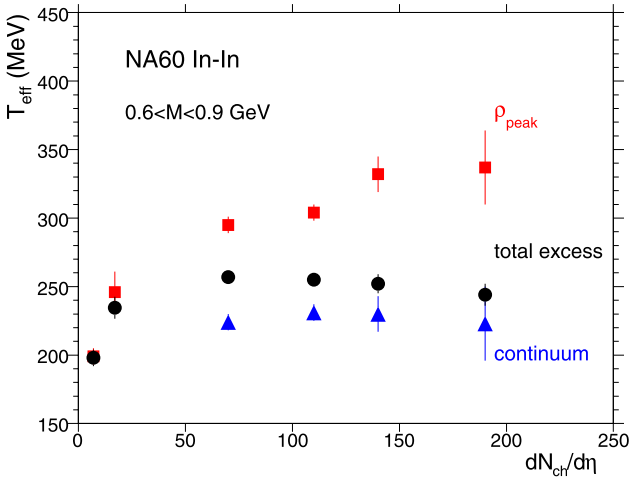

Fig. 5.1 Inverse slope parameter $T_{\rm eff}$ vs. centrality for continuum, peak and total in the mass window $0.6 < M < 0.9$ GeV (see also 4.1, *right*). *Open charm* is subtracted throughout

with processes like $q\bar{q} \to \mu^+\mu^-$, for which flow has not yet built up [19, 23]. In this sense, the present analysis may well represent the first data-based evidence for thermal radiation of partonic origin in nuclear collisions, overcoming parton–hadron duality in the yield description on the basis of M–p_T correlations as discussed in Sect. 3.

Theoretically, the extension of the unified LMR and IMR results over the complete M–p_T plane places severe constraints on the dynamical trajectories of the fireball evolution. Indeed all present scenarios [18, 19, 23, 26, 27] do not any longer rely on parton–hadron duality in the rates as in [21], but explicitly differentiate between hadronic (mostly 4π) and partonic contributions in the IMR as already discussed in connection with Fig. 2.3. The partonic fraction presently ranges from 0.65 for [26] (option EoS-B$^+$ as used in Fig. 4.1) to "dominant" in [19, 23, 27]. The exponential shape of the experimental m_T spectra is reproduced by the models, consistent with the expectations for thermal radiation. However, due to remaining uncertainties in the equation-of-state, in the fireball evolution and in the role of hard processes [26], a quantitative description of the much more sensitive m_T-derivative $T_{\rm eff}$ vs. M in Fig. 4.5 is only slowly emerging. In particular, the more recent results from the authors of [19, 23, 27], while very encouraging in the description of the downward jump, are still preliminary and have not yet been formally published in their final form. A systematic comparison of several model results to the data in Fig. 4.5 is therefore presently not possible.

5 Centrality dependencies

All data presented so far correspond either to (nearly) minimum bias, selecting $\mathrm{d}N_{\rm ch}/\mathrm{d}\eta > 30$, or to the semicentral window, selecting $110 < \mathrm{d}N_{\rm ch}/\mathrm{d}\eta < 170$; the results for the two conditions are very close. However, an enormous amount of information exists on the centrality dependence of practically every variable discussed in this paper. We select two topics of particular relevance here.

The first one concerns the evolution of the shape of the excess mass spectra, following Figs. 2.2 and 2.3. In [15], we have used both an *rms* analysis and a more sensitive side-window method to determine separately the yields of the peak and the underlying continuum. The centrality dependence from the latter is shown in Fig. 4.6: peak, continuum and total excess yield in the mass interval $0.2 < M < 1.0$ GeV, all normalized to the (fictitious) cocktail ρ with the assumption $\rho/\omega = 1$ (like in pp). The ω itself is directly measured, and its yield is found to be proportional to $\mathrm{d}N_{\rm ch}/\mathrm{d}\eta$. The continuum and the total show a very strong increase, starting already in the peripheral region, while the peak slowly decreases from >1 to <1. Recalling that Fig. 4.6 is based on the excess mass spectra before acceptance correction like in Fig. 2.3, roughly representing the full ρ spectral function, the excess/ρ ratio can directly be interpreted as the number of ρ generations created by formation and decay during the fireball evolution, including freeze-out: the "ρ clock", frequently discussed in the past. It reaches up to about 6 generations for central In–In collisions; selecting low p_T this number doubles.

The second topic concerns the centrality dependence of the slope parameter $T_{\rm eff}$ for the excess data in the ρ-like window $0.6 < M < 0.9$ GeV, following Fig. 4.1 (right). Based as before on the side-window method [15], the results are shown in Fig. 5.1, separately for the ρ peak, the continuum and the total excess. The peak is seen to show a very strong rise, with hardly any saturation. However, the errors in the more central data become quite large, reflecting the continu-

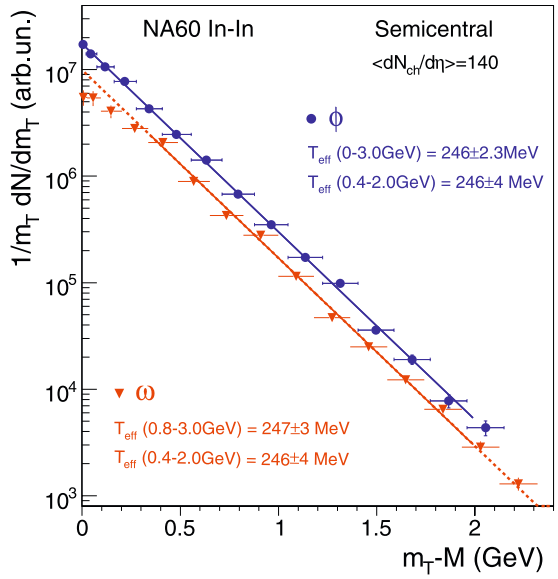

Fig. 5.2 Acceptance-corrected transverse mass spectra of the ω and the ϕ for the semicentral bin. The $T_{\rm eff}$ values correspond to different fit ranges for the two particles. A depletion of the ω yield at low m_T relative to the fit line can clearly be recognized

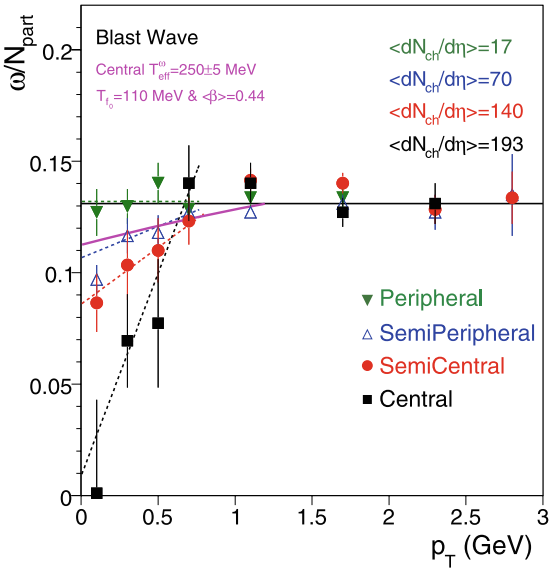

Fig. 6.1 p_T dependence of the ω yield with respect to the fit line in Fig. 5.2, absolutely normalized for the full phase space yield, for different centralities. The *solid line* for $p_T \leq 1$ GeV shows the result from a blast-wave fit to the ω for central collisions. The *dotted lines* are only meant to guide the eye. The errors are purely statistical. The systematic errors are negligibly small compared to the statistical ones

ously decreasing peak/total ratio as visible in Fig. 4.6. Conversely, continuum and total yield saturate much earlier.

The large gap in $T_{\rm eff}$ between the peak and the continuum, seen already in Fig. 4.4, has a much-debated interesting physics origin. The p_T spectrum of a thermal in-medium source is softer by a Lorentz factor $M/E{=}1/\gamma$ compared to that of a freely decaying freeze-out ρ [26]. On top, the in-medium values of $T_{\rm eff}$ represent a temperature-flow average, while the freeze-out ρ receives the maximal flow. These two effects contribute about equally to the total. The size of the gap ultimately reaches 70–100 MeV, but closes towards peripheral collisions. The ω, with the same mass as the ρ, also shows a large gap to the ρ (compare Fig. 5.2), which also closes finally to zero for the lowest pp-like window [13].

6 Evidence for ω in-medium modifications

While most of the historical discussion on light-flavor vector mesons in hot and dense matter has concentrated on the short-lived ρ ($c\tau = 1.3$ fm), the longer-lived ω (23 fm) and ϕ (46 fm) have received much less attention, since most of their dilepton decays occur after thermal freeze-out. Within the NA50 LMR analysis, the ω and ϕ have indeed consistently been treated as "cocktail" particles and subtracted from the total (compare Fig. 2.1). However, in-medium effects are expected for the (small) decay fraction inside the fireball, and these are actually contained in the Hees/Rapp scenario (see [26] and earlier references in there).

NA60 has addressed the ω in a way directly coupled to the cocktail subtraction procedure. Due to the high mass resolution, the *disappearance* of the yield at low p_T out of the narrow ω peak in the nominal pole position can sensitively be detected. The *appearance* of the yield elsewhere in the mass spectrum, originating from a mass shift, or broadening or both, is practically unmeasurable, due to the masking of the whole region by the much stronger $\pi\pi \rightarrow \rho$ process, regenerating the ρ. Sensitive experiments on ω in-medium effects with clear clues as to their characteristics can therefore only be done in cold nuclear matter experiments [29], where $\rho/\omega = 1$, but not in ultra-relativistic nuclear collisions. The evidence for the disappearance of ω's in the low m_T region is shown in Fig. 5.2.

As already mentioned in Sect. 2, the ω and ϕ are obtained as a byproduct of the cocktail subtraction procedure. The data are fit with the usual m_T exponential used before in Figs. 4.1 and 4.3. With respect to this reference line, there is hardly any anomaly visible for the ϕ, but quite some loss for low-p_T ω's. The loss can be quantified with respect to the reference line, extrapolating down to zero. The fit parameters $T_{\rm eff}$ for two different fit regions both for the ω and the ϕ show the definition of the reference line to be quite uncritical. Forming the ratio data/reference line takes care of that part of radial flow which does not seriously affect the exponential slope.

The results are shown in Fig. 6.1, absolutely normalized as the full phase space ratio $\omega/N_{\rm part}$. The effects of ω disappearance are quite striking: (i) a suppression of the relative

yield below the reference line only occurs for $p_T \leq 1$ GeV; (ii) there is a very strong centrality dependence of the suppression, reaching down to $\leq$0.5 of the reference line (the errors become huge for the central window, because the ω can then hardly be recognized on top of the $\pi\pi$ processes at low m_T); (iii) the suppression effects are much larger than expected for the spectral distortions due to the blue shift from radial flow at low m_T; a simulation in the basis of the blast wave parameters from [14] shows at most 10% effects for central collisions. Theoretical simulations addressing these results are not yet available. It should be added that the same procedure applied to the ϕ does describe the data solely on the basis of radial flow. No effect beyond that can be recognized, within errors.

7 Conclusions

This paper, supplementing [14], contains the most comprehensive data set on excess dileptons above the known sources which has so far become available through NA60. We have concentrated here more than before on interpretational aspects, in particular on the way, "parton–hadron duality" in the yields can be overcome by a careful study of M–p_T correlations. The data mediate a clear conclusion on the dominance of partonic processes for $M > 1$ GeV. A systematic comparison with theoretical models reveals remaining ambiguities in the modeling, but the overall agreement with the data tends by now to support the same conclusion.

References

1. R.D. Pisarski, Phys. Lett. B **110**, 155 (1982)
2. R. Rapp, J. Wambach, Adv. Nucl. Phys. **25**, 1 (2000)
3. G.E. Brown, M. Rho, Phys. Rept. **363**, 85 (2002)
4. L.D. McLerran, T. Toimela, Phys. Rev. D **31**, 545 (1985)
5. K. Kajantie, M. Kataja, L.D. McLerran, P.V. Ruuskanen, Phys. Rev. D **34**, 811 (1986)
6. G. Agakichiev et al. (CERES Collaboration), Eur. Phys. J. C **41**, 475 (2005), and earlier references therein
7. D. Adamova et al. (CERES Collaboration), Phys. Lett. B **666**, 425 (2008)
8. M.C. Abreu et al. (NA38/NA50 Collaboration), Nucl. Phys. A **698**, 539 (2002), and earlier reference
9. A.L.S. Angelis et al. (HELIOS-3 Collaboration), Eur. Phys. J. C **13**, 433 (2000), and earlier reference
10. H.J. Specht, Nucl. Phys. A **805**, 338 (2008). arXiv:0710.5433 [nucl-ex]
11. R. Arnaldi et al. (NA60 Collaboration), Eur. Phys. J. C (2008, to be published). arXiv:0810.3204 [nucl-ex]
12. R. Arnaldi et al. (NA60 Collaboration), Phys. Rev. Lett. **96**, 162302 (2006)
13. R. Arnaldi et al. (NA60 Collaboration), Phys. Rev. Lett. **100**, 022302 (2008)
14. S. Damjanovic et al. (NA60 Collaboration), J. Phys. G **35**, 104036 (2008). arXiv:0805.4153 [nucl-ex]
15. S. Damjanovic et al. (NA60 Collaboration), Eur. Phys. J. C **49**, 235 (2007)
16. R. Rapp, (2003), private communication and R. Rapp, nucl-th/0204003
17. M. Harada, C. Sasaki, Int. J. Mod. Phys. E **16**, 2143 (2007). hep-ph/0702205
18. H. van Hees, R. Rapp, Phys. Rev. Lett. **97**, 102301 (2006). hep-ph/0603084
19. J. Ruppert, C. Gale, T. Renk, P. Lichard, J.I. Kapusta, Phys. Rev. Lett. **100**, 162301 (2008). hep-ph/0706.1934
20. V.L. Eletsky, M. Belkacem, P.J. Ellis, J.I. Kapusta, Phys. Rev. C **64**, 035202 (2001)
21. R. Rapp, E.V. Shuryak, Phys. Lett. B **473**, 13 (2000)
22. G.Q. Li, C. Gale, Phys. Rev. C **58**, 2914 (1998)
23. T. Renk, J. Ruppert, Phys. Rev. C **77**, 024907 (2008). hep-ph/0612113
24. S. Damjanovic et al. (NA60 Collaboration), Nucl. Phys. A **783**, 327 (2007)
25. M. Floris et al. (NA60 Collaboration), J. Phys. G **35**, 104054 (2008). arXiv:0809.0420 [hep-ex]
26. H. van Hees, R. Rapp, Nucl. Phys. A **806**, 339 (2008)
27. K. Dusling, D. Teaney, I. Zahed, Phys. Rev. C **75**, 024908 (2007). hep-ph/0701253
28. E.L. Bratkovskaya, W. Cassing, O. Linnyk, arXiv:0805.3177 [nucl-th]
29. M. Kotulla et al. (CBELSA/TAPS Collaboration), Phys. Rev. Lett. **100**, 192302 (2008)